Journal of Applied Fluid Mechanics, Vol. 9, No. 5, pp. 2141-2147, 2016.
Available online at www.jafmonline.net, ISSN 1735-3572, EISSN 1735-3645.
DOI: 10.18869/acadpub.jafm.68.236.24429

Stability of Unsteady Mixed Convection in a Horizontal Concentric Annulus

K. Kahveci

Trakya University, Department of Mechanical Engineering, 22180 Edirne, Turkey

Email: kamilk@trakya.edu.tr

(Received December 27, 2014; accepted January 1, 2016)

ABSTRACT

In this study, stability of unsteady mixed convection in a horizontal annulus between two concentric cylinders was investigated numerically. The surfaces of the cylinders were considered to be at fixed temperatures and it was assumed that the hot inner cylinder is rotating at a constant angular velocity. The buoyancy forces were formulated utilizing the Boussinesq approximation. The governing equations of fluid flow and heat transfer in the annulus were solved with a finite element method for different values of the geometric (radius ratio) and transport parameters (Rayleigh number and Reynolds number). Development of the convective flow and heat transfer was expressed by the average Nusselt number for the outer cylinder. The results show that, for a narrow gap annulus, convective flow induces flow bifurcation and becomes unstable for high values of the Rayleigh number. Flow becomes more unstable with an increase in the Reynolds number. For a wide gap annulus, flow is stable for all values of the Rayleigh number if the rotation effects are small. On the other hand, convective flow becomes unstable for the modest and high values of the Ra number with an increase in the Re number.

Keywords: Mixed convection; Concentric annulus; Stability; Bifurcation; Nusselt number; Rayleigh number.

NOMENCLATURE

g	gravitational acceleration
k	thermal conductivity
L	characteristic length, $L=R_o-R_i$
NE	number of elements
Nu	Nusselt number
n	Index in
P	pressure
Pr	Prandtl number
q	local heat flux
R	radius
Ra	Rayleigh number
Re	Reynolds number
RR	radius ratio, $RR=R_o/R_i$
r	radial coordinate
SR	spatial resolution
T	temperature
t	time
u	radial velocity component
v	angular velocity component
α	thermal diffusivity
β	thermal expansion coefficient
ν	kinematic viscosity
θ	angular coordinate
ρ	density
Ω	angular velocity
Subscripts	
a	average
c	cold
h	hot
i	inner cylinder
o	outer cylinder
Superscripts	
*	dimensional variable
Overlines	
–	time-averaged

1. INTRODUCTION

Convective heat transfer between the two horizontal concentric cylinders has been focus of many studies due to its wide range of applications such as heat exchangers, solar collectors, nuclear reactors, thermal energy storage systems and electronic devices. Previous investigations have generally focused on natural convection and on the effects of pertinent parameters on flow and heat transfer. Kuehn and Goldstein (1976a, 1978) investigated the effects of Rayleigh and Prandtl numbers and aspect ratio on flow and heat transfer, Kuehn and

Goldstein (1976b) and Fattahi *et al*. (2010) conducted an experimental and theoretical study on the effects of eccentricity of the cylinders on natural convection. Ashorynejad *et al*. (2013) studied the effects of magnetic field on natural convective flow and heat transfer. Shaija and Narasimham (2009) conducted a numerical investigation on the effects of surface radiation on natural convection heat transfer. Abu-Nada *et al*. (2008) studied the effects of nanofluid usage on natural convection. There are also several studies on mixed convection in the literature, although limited in numbers. Yang and Farouk (1992) investigated the mixed convection in a horizontal annulus with a heated rotating inner cylinder for a wide range of governing parameters. Khanafer and Chamka (2003) examined mixed convection within a horizontal annulus and found that the Richardson number plays a significant role on heat transfer characteristics within the annulus. Yoo (1998) investigated mixed convection between two horizontal concentric cylinders with a cooled rotating outer cylinder and concluded that heat transfer decreases as the Reynolds number increases.

Under certain conditions, annular flow shows a multiplicity of solutions called the bifurcation phenomenon associated with the hydrodynamic and/or thermal instabilities (Chung *et al*. 1999). Bifurcative natural convection in a horizontal concentric annulus was investigated by Chung *et al*. (1999). It was found that the instability is thermal for high critical Rayleigh number and the hydrodynamic instability is compatible with the thermal instability for moderate critical Rayleigh number. In another study, Yu *et al*. (2012) observed that more stable flow patterns are seen for a relatively wide-gap annulus; on the contrary, convective flow in a narrow-gap annulus tends to induce flow bifurcation and to become unstable.

As it can be seen from the aforementioned studies, the majority of the studies are on steady-state characteristics of the convective flow and heat transfer in an annulus. However, knowledge on the transient character of the problem, which carries great practical importance, is quite limited. Therefore, effects of pertinent parameters on the stability of unsteady mixed convective flow in a horizontal concentric annulus were investigated numerically in this study.

2. ANALYSIS

Geometry and coordinate system used in the study is seen in Fig. 1. The radius of the inner cylinder at temperature T_h is R_i, while the radius of the cold outer cylinder at T_c is R_o. The fluid in the annulus is initially stagnant and its temperature is equal to the temperature of the outer cylinder. It was assumed that the temperature of the inner cylinder is suddenly (at t=0) increased and maintained at this temperature. Taylor vortices were assumed not to develop in the annulus. The governing equations were derived under the assumptions that the flow is two dimensional and laminar, the fluid is incompressible and has constant thermophysical properties. The buoyancy forces were assumed to be expressed using the Boussinesq approximation. The governing equations can then be written in a non-dimensional form as follows:

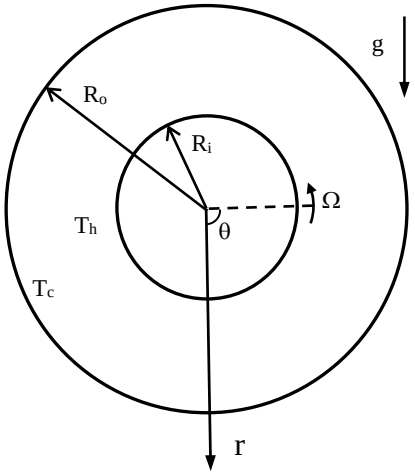

Fig. 1. Geometry and coordinate system.

$$\frac{\partial u}{\partial r}+\frac{u}{r}+\frac{1}{r}\frac{\partial v}{\partial \theta}=0 \tag{1}$$

$$\frac{\partial u}{\partial t}+u\frac{\partial u}{\partial r}+\frac{v}{r}\frac{\partial u}{\partial \theta}-\frac{v^2}{r}=-\frac{\partial P}{\partial r}+\frac{1}{\mathrm{Re}}\left[\frac{\partial}{\partial r}\left(\frac{1}{r}\frac{\partial (ur)}{\partial r}\right)+\frac{1}{r^2}\frac{\partial^2 u}{\partial \theta^2}-\frac{2}{r^2}\frac{\partial v}{\partial \theta}\right]+\frac{Ra}{\mathrm{Pr}\,\mathrm{Re}^2}T\cos\theta \tag{2}$$

$$\frac{\partial v}{\partial t}+u\frac{\partial v}{\partial r}+\frac{v}{r}\frac{\partial v}{\partial \theta}+\frac{vu}{r}=-\frac{1}{r}\frac{\partial P}{\partial \theta}+\frac{1}{\mathrm{Re}}\left[\frac{\partial}{\partial r}\left(\frac{1}{r}\frac{\partial (vr)}{\partial r}\right)+\frac{1}{r^2}\frac{\partial^2 v}{\partial \theta^2}+\frac{2}{r^2}\frac{\partial u}{\partial \theta}\right]+\frac{Ra}{\mathrm{Pr}\,\mathrm{Re}^2}T\sin\theta \tag{3}$$

$$\frac{\partial T}{\partial t}+u\frac{\partial T}{\partial r}+\frac{v}{r}\frac{\partial T}{\partial \theta}-=\frac{1}{\mathrm{Re}\,\mathrm{Pr}}\left[\frac{1}{r}\frac{\partial}{\partial r}\left(r\frac{\partial T}{\partial r}\right)+\frac{1}{r^2}\frac{\partial^2 T}{\partial \theta^2}\right] \tag{4}$$

where u and v are the dimensionless radial and angular velocity, and P is the dimensionless pressure. The dimensionless parameters, Prandtl, Reynolds and Rayleigh numbers are defined as:

$$\mathrm{Pr}=\frac{\nu}{\alpha},\ \mathrm{Re}=\frac{\Omega R_i L}{\nu},\ Ra=\frac{g\beta(T_h-T_c)L^3}{\nu\alpha} \tag{5}$$

where ν, α, Ω, β are the kinematic viscosity, thermal diffusivity, angular velocity, and the thermal expansion coefficient, respectively. L is the characteristic length chosen as the gap between the two cylinders, i.e., $L=R_o-R_i$. The following dimensionless variables are used in the nondimensionalization of the governing equations:

$$r = \frac{r^*}{L},\ u = \frac{u^*}{\Omega R_i},\ v = \frac{v^*}{\Omega R_i},$$
$$P = \frac{1}{\rho(\Omega R_i)^2} v^*,\ t = \frac{t^*}{L/(\Omega R_i)} \quad (6)$$

The governing equations are subjected to the following initial and boundary conditions:

$$u = 0,\ v = 0,\ T = 0 \ at\ \ t = 0 \quad (7)$$

$$u = 0,\ v = 1,\ T = 1 \ at\ \ r = R_i / L \quad (8)$$

$$u = 0,\ v = 0,\ T = 0 \ at\ \ r = R_o / L \quad (9)$$

Nusselt number is one of the most important dimensionless parameters in convective heat transfer. The local Nusselt number for the outer cylinder can be defined as:

$$Nu = R_o \ln \frac{R_o}{R_i} \frac{qL}{k(T_h - T_c)} \quad (10)$$

where q is the local heat flux and k is the thermal conductivity of the fluid. The average Nusselt number can then be expressed as:

$$Nu_a = \frac{1}{2\pi} \int_0^{2\pi} Nu d\theta \quad (11)$$

The overall heat transfer during the course of flow development can be presented by the time-averaged Nusselt number defined as:

$$\overline{Nu}_a = \frac{1}{t_{total}} \int_0^{t_{total}} Nu_a dt \quad (12)$$

where t_{total} is the total time duration.

3. RESULTS AND DISCUSSION

The governing equations presented in the previous section were iteratively solved with a finite element modelling and simulation software (Comsol 4.2). The domain was meshed with triangular mesh elements. The temporal and spatial terms in the governing equations were discretized using a second-order implicit scheme. Absolute convergence criteria were selected as 10^{-4} for the velocities and 10^{-6} for the temperature. In order to verify the accuracy of the results, the average Nu numbers obtained in this study for the natural convection were compared with the correlation results developed by Yu *et al.* (2012). As it can be seen in Table 1, there is a good agreement between the results. In this study, a test was also conducted for the selection of spatial and temporal resolutions suitable for a certain accuracy of the solution. In this test, 3 different cell numbers and 2 different time-step intervals were considered, as it can be seen in Table 2. For each case, relative deviation was given with reference to the fine spatial and temporal resolutions. The results show that the relative deviation is smaller if the centrifugal forces are at important levels (Re=100). The relative deviation is at 3% for the coarse grid resolution. The deviation gets smaller values than 1% if the spatial resolution is normal. Additionally, when a normal spatial resolution is used, results become insensitive to the time-step interval. Using a smaller time-step interval provides only a 0.2% decrease in the relative deviation. Considering the results given in Table 2, a fine spatial resolution and a time-step interval of $5x10^{-4}$ for Re=1 and a time-step interval of $5x10^{-2}$ for the Re=100 were used in this study.

The flow and heat transfer in the annulus were investigated for three different values of the Rayleigh number (Ra= 10^4, 10^5, and 10^6) in this study. The radius ratio, RR, was selected as 1.5 for the narrow gap annulus and RR=3.0 for the wide gap annulus. Two different values of the Reynolds number were considered (Re=1 and 100). The Prandtl number was fixed at Pr=7.0, and the computations were performed up to a time duration of t=3 for the Re=1 and t=300 for the Re=100. Relative importance of the buoyancy and centrifugal forces to one another is determined by the Richardson number described as $Ri=Gr/Re^2$. Typically, the buoyancy forces are negligible if Ri<0.1, centrifugal forces are negligible if Ri>10, and neither are negligible if 0.1<Ri<10.

Table 1 Comparison of the time-averaged Nusselt numbers along the outer cylinder for natural convection

RR	Ra	Yu *et al.* (2012)	Present Study
1.5	10^4	1.34	1.32
	10^5	2.49	2.48
	10^6	4.64	4.60
3.0	10^4	1.26	1.25
	10^5	2.16	2.12
	10^6	3.73	3.68

Table 2 The time-averaged Nusselt numbers for different combinations of spatial and temporal resolutions (RR =3.0 and Ra = 10^6).

Re	SR	NE	Δt	$\overline{Nu}_a$	Dv. %
1	Coarse	6078	$1x10^{-3}$	3.343	3.00
	Normal	20316	$1x10^{-3}$	3.449	0.87
	Normal	20316	$5x10^{-4}$	3.449	0.84
	Fine	48834	$5x10^{-4}$	3.446	0.00
100	Coarse	6078	$1x10^{-1}$	3.324	1.21
	Normal	20316	$1x10^{-1}$	3.389	0.74
	Normal	20316	$5x10^{-2}$	3.383	0.55
	Fine	48834	$5x10^{-2}$	3.365	0.00

The development of convective flow and heat transfer was presented by the average Nusselt number along the outer cylinder in this study. The evolution of the average Nusselt number along the outer cylinder is seen in Fig. 2 for the narrow gap annulus (RR=1.5) and Re=1. Until the fluid particles heated through the inner hot cylinder reach the outer cylinder, the temperature gradient does not develop on the outer cylinder, and therefore the average Nusselt number is zero at the initial stage of the flow as it can be seen in Fig. 2. This stage becomes shorter with the increase of the Rayleigh number depending on the stronger natural convection currents. After this initial stage, a sudden increase in the average Nu number is seen

due to the developing thermal gradient. Increasing trend in the average Nu number continues at a modest level until the steady state flow condition is reached. In high Ra numbers, the average Nu number exhibits an oscillatory behavior, following a primary overshoot, due to the flow bifurcation as the convective flow is unstable. Similar trend in the average Nu number was also observed by Yu *et al*. (2012). The results for the Re=100 are given in Fig. 3. The centrifugal forces are dominant for the $Ra=10^4$, both buoyancy forces and centrifugal forces are important for the $Ra=10^5$, and buoyancy forces are dominant for the $Ra=10^6$. As it can be seen in Fig. 3, a decrease in the average Nu number is observed with an increase in the Reynolds number as the centrifugal forces are dominant over buoyancy forces. From the comparison of Figs. 2 and 3, it can be observed that the amplitude of the oscillations gets higher values with increasing Re number. This shows that the convective flow becomes more unstable with an increase in the Re number. Similar behavior was also observed in the study performed by Choi and Kim (1995).

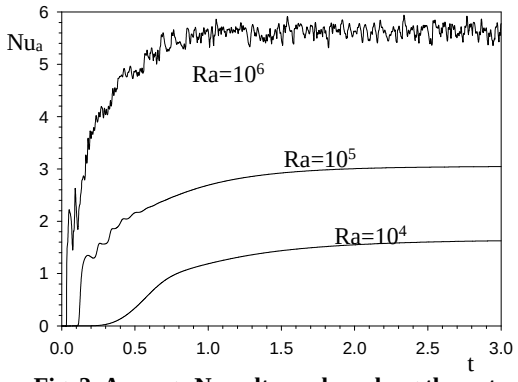

Fig. 2. Average Nusselt number along the outer cylinder for RR=1.5 and Re=1.

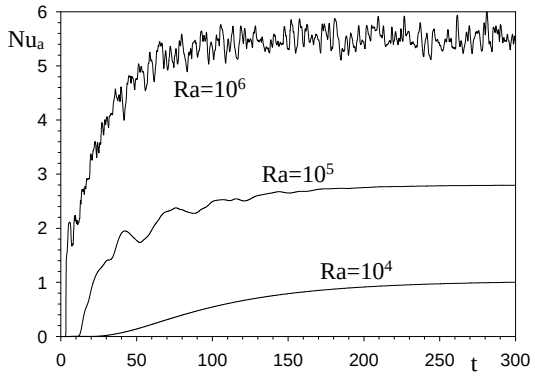

Fig. 3. Average Nusselt number along the outer cylinder for RR=1.5 and Re=100.

The evolution of the average Nusselt number along the outer cylinder is seen in Fig. 4 for the wide gap annulus (RR=3.0) and Re=1. As opposed to the flow in the narrow gap annulus, convective flow is stable and steady state is attained after the developing stage for all values of the Ra number. The overshoots in the early stage of the flow are still exist, but their span and altitude get smaller values. As it can be seen in Fig. 5, convective flow is unstable for high values of the Rayleigh number for the Re=100. As the Reynolds number increases, flow becomes unstable as the rotation of the inner cylinder contributes instabilities when the buoyancy forces are at important levels. Flow is also unstable for the $Ra=10^5$ as opposed to the flow in the narrow annulus as the viscous forces contributing flow stability are less effective for the wide gap annulus. Furthermore, oscillation period gets higher values and a more regular oscillatory behavior is observed for the $Ra=10^5$ with respect to $Ra=10^6$.

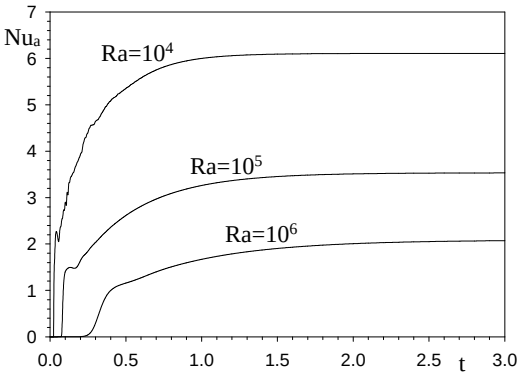

Fig. 4. Average Nusselt number along the outer cylinder for RR=3.0 and Re=1.

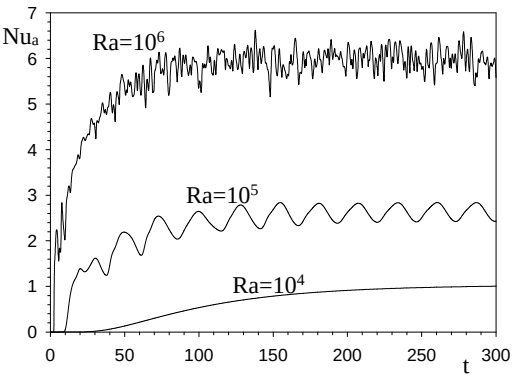

Fig. 5. Average Nusselt number along the outer cylinder for RR=3.0 and Re=100.

The streamlines and isotherms at a final stage of the flow are seen in Fig. 6 for the RR=1.5 and Re=1. The centrifugal forces are at negligible levels due to the low Reynolds number and the flow is formed with the natural convection currents as a result of the buoyancy forces. The heated fluid particles ascend along the inner cylinder until they reach the outer cylinder. Then they move downward along the outer cylinder while they are cooled. Their flow paths are completed as the colder fluid particles are entrained to the ascending fluid particles. As a result, cellular flow structures form on the left and right regions of the annulus. Convective flow is weak and viscous forces are dominant over the buoyancy forces for the $Ra=10^4$. Therefore, heat transfer is conduction-dominant and isotherms are almost in circular pattern in accordance with the circumference curves of the inner and outer

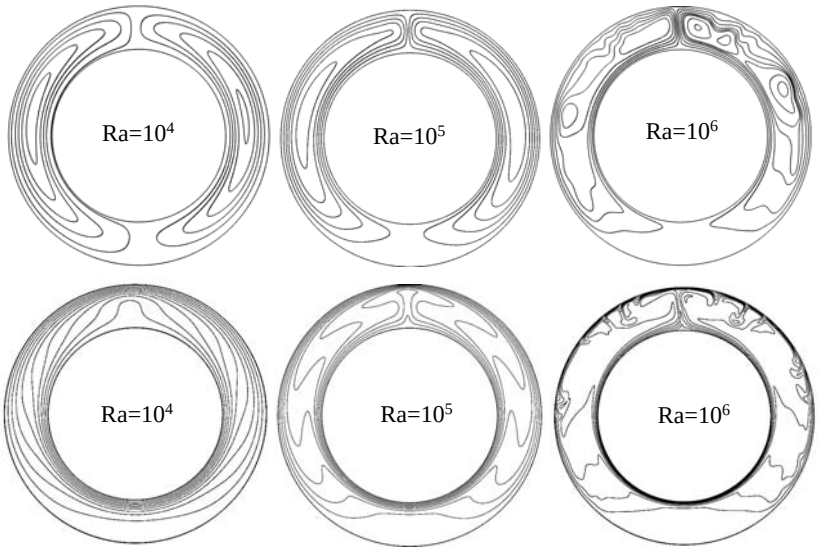

Fig. 6. Streamlines (top) and isotherms (bottom) for RR=1.5 and Re=1.

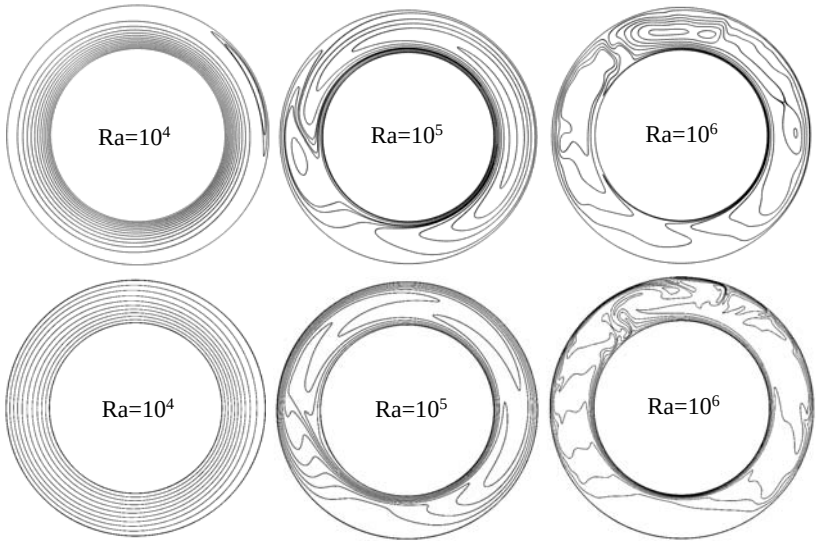

Fig. 7. Streamlines (top) and isotherms (bottom) RR=1.5 and Re=100.

cylinders. Flow evolves into boundary layer flow regime with the increasing Ra number depending on the high strength of convection. Thus, plateau formations are seen in the isotherms at the core region of the annulus for high Ra numbers. As it can also be seen from Fig. 6 that flow and heat transfer patterns are nearly symmetrical for the stable flow at $Ra=10^4$ and $Ra=10^5$. Although the locations of the recirculating cells on the left and right region of the annulus exhibit asymmetry about the vertical symmetric line, the isotherms are symmetrical on both regions. For the $Ra=10^6$, the symmetry breaks down as the flow becomes unstable due to the presence of multicellular flow structure. In this flow regime, fluid particles on the upper part of the annulus no longer ascends vertically along the symmetry line and shifts to the left, which indicates the presence of flow bifurcation.

The streamlines and isotherms are seen in Fig. 7 for the RR=1.5 and Re=100. The centrifugal forces are dominant for the $Ra=10^4$. Therefore, the streamlines and isotherms are nearly in circular patterns. A clockwise rotating cellular structure emerges with the effect of natural convection currents on the top right corner of the annulus. For the $Ra=10^5$, both the centrifugal and buoyancy forces are in important levels. The heated flow particles along the inner cylinder on the left part of the annulus are carried to the right of the annulus with the effect of the centrifugal forces. Then they are shifted to the right and begin to move upwards by the effect of buoyancy forces until they reach the top of the outer cylinder. Finally, they begin to descend along the cold outer cylinder and complete their flow paths. This cellular flow structure encompasses around 2/3rds of the annulus. A secondary cellular flow develops on the lower left part of the annulus. The heated flow particles on this region move upwards. However, due to the other circular flow, they are shifted to the left towards the outer cylinder and

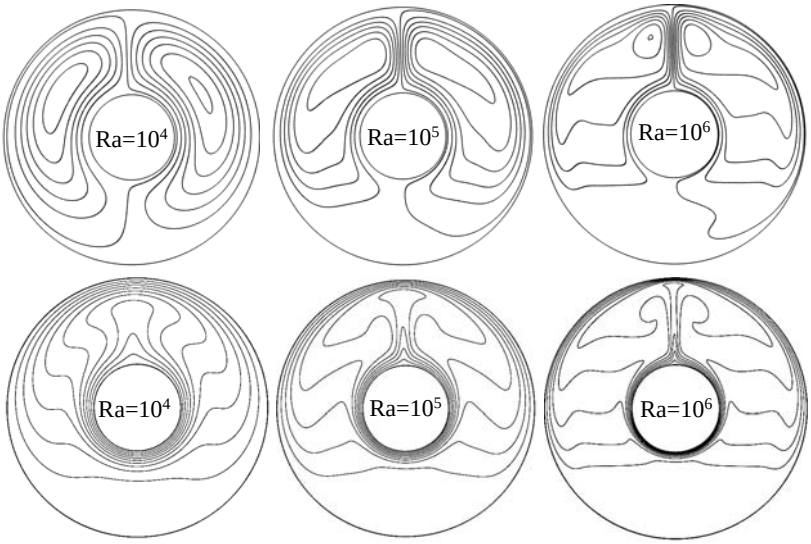

Fig. 8. Streamlines (top) and isotherms (bottom) for RR=3.0 and Re=1.

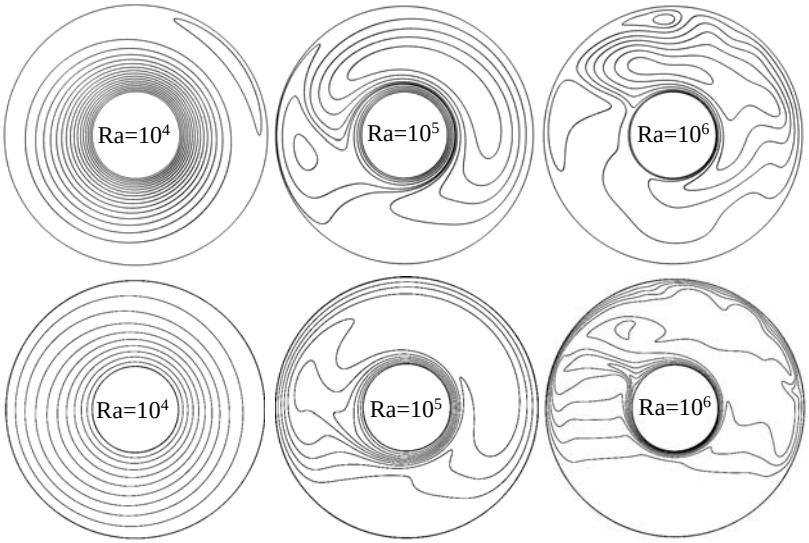

Fig. 9. Streamlines (top) and isotherms (bottom) for RR=3.0 and Re=100.

then move downwards and complete the flow paths. As it can be observed from the isotherms, the relatively cold area at the bottom of the annulus is shifted to the left due to this flow structure. For the $Ra=10^6$, flow is unstable and a multicellular flow is present for both the left and the right regions of the annulus. The place where the flow particles shift towards the outer wall on the left region is closer to the symmetry axis as the buoyancy forces are dominant.

The streamlines and isotherms are seen in Fig. 8 for the RR=3.0 and Re=1. Similar to the narrow gap annulus, cellular flow is present on both side of the annulus. The cells rotate clockwise on the right region of the annulus, while the cells rotate counter-clockwise on the left region of the annulus. Flow and heat transfer patterns are nearly symmetrical for all the Rayleigh numbers. This indicates that the flow is stable and develops towards a steady state flow regime.

The streamlines and isotherms are seen in Fig. 9 for the RR=3.0 and Re=100. For the $Ra=10^4$ and $Ra=10^5$, flow and heat transfer patterns are similar to those of the narrow gap annulus. For the $Ra=10^6$, cellular flow is present on the right and left regions of the annulus. These flow patterns are similar to those of the $Ra=10^5$. However, a third circular flow develops on the upper region of the annulus for the $Ra=10^6$. As it was stated before, rotation of the inner cylinder tends to induce flow bifurcation when the buoyancy effects are important. As a result, convective flow is unstable for the $Ra=10^5$ and $Ra=10^6$.

4. CONCLUSION

In this study, stability of unsteady mixed convection in a horizontal annulus between two concentric

cylinders was investigated numerically. The concluding remarks are: convective flow induces flow bifurcation and becomes unstable for a narrow gap annulus as the Ra number increases. Flow becomes more unstable with an increase in the Reynolds number. For a wide gap annulus, flow is stable for all values of the Rayleigh number when the centrifugal effects are small. On the other hand, convective flow becomes unstable for modest and high values of the Rayleigh number with an increase in the Reynolds number.

REFERENCES

Abu-Nada, E., Z. Masoud and A. Hijazi (2008). Natural convection heat transfer enhancement in horizontal concentric annuli using nanofluids. *International Communications in Heat and Mass Transfer* 35, 657–665.

Ashorynejad, H. R., A. A. Mohamad and M. Sheikholeslami (2013). Magnetic field effects on natural convection flow of a nanofluid in a horizontal cylindrical annulus using Lattice Boltzmann method. *International Journal of Thermal Sciences* 64, 240-250.

Choi, J. Y. and M.-U. Kim (1995). Three-dimensional linear stability of mixed convective flow between rotating horizontal concentric cylinders. *International Journal of Heat and Mass Transfer* 38(2), 275-285.

Chung, J. D., C.-J. Kim, H. Yoo and J. S. Lee (1999). Numerical investigation on the bifurcative natural convection in a horizontal concentric annulus. *Numerical Heat Transfer, Part A: Applications* 36(3), 291–307.

Fattahi, E., M. Farhadi and K. Sedighi (2010). Lattice Boltzmann simulation of natural convection heat transfer in eccentric annulus. *International Journal of Thermal Sciences* 49(1), 2353-2362.

Khanafer, K. and A. J. Chamkha (2003). Mixed convection with in a porous heat generating horizontal annulus. *International Journal of Heat and Mass Transfer* 46(10), 1725-1735.

Kuehn, T. H. and R. Goldstein (1978). A parametric study of Prandtl number and diameter ratio effects on natural convection heat transfer in horizontal cylindrical annuli. *Journal of Heat Transfer* 102(4), 768–770.

Kuehn, T. H. and R. J. Goldstein (1976a). Correlating equations for natural convection heat transfer between horizontal circular cylinders. *International Journal of Heat and Mass Transfer* 19(10), 1127–1134.

Kuehn, T. H. and R. J. Goldstein (1976b). An experimental and theoretical study of natural convection in the annulus between horizontal concentric cylinders. *Journal of Fluid Mechanics* 74(4), 695-719.

Shaija, A. and G. S. V. L. Narasimham (2009). Effect of surface radiation on conjugate natural convection in a horizontal annulus driven by inner heat generating solid cylinder. *International Journal of Heat and Mass Transfer* 52(5-6), 5759–5769.

Yang, L. and B. Farouk (1992). Three-dimensional mixed convection flows in a horizontal annulus with a heated rotating inner circular cylinder. *International Journal of Heat and Mass Transfer* 35(8), 1947-1956.

Yoo, J. S. (1998). Mixed convection of air between two horizontal concentric cylinders with a cooled rotating outer cylinder. *International Journal of Heat and Mass Transfer* 41(2), 293-302.

Yu, Z. T., X. Xu, Y. C. Hu, L. W. Fan and K. F. Cen (2012). A numerical investigation of transient natural convection heat transfer of aqueous nanofluids in a horizontal concentric annulus. *International Journal of Heat and Mass Transfer* 55(4), 1141–1148.